Supplementary Information

Field-Tailoring Quantum Materials via Magneto-Synthesis: Metastable Metallic and Magnetically Suppressed Phases in a Trimer Iridate

Tristan R. Cao[1], Hengdi Zhao[1], Xudong Huai[2], Arabella Quane[1], Thao T. Tran[2], Feng Ye[3] and Gang Cao[1]

[1]Department of Physics, University of Colorado at Boulder, Boulder, CO 80309

[2]Department of Chemistry, Clemson University, Clemson, SC 29634

[3]Oak Ridge National Laboratory, Oak Ridge, TN 37830

I. Experimental Details

Single crystals studied were grown using a flux method. The mixtures were fired at 1300 °C for 15-20 hours and then slowly cooled to room temperature at a rate of 3 C/hour. Platinum crucibles were used. Measurements of crystal structures were performed using a Bruker Quest ECO single-crystal diffractometer. It is equipped with an Oxford Cryosystem that creates sample temperature environments ranging from 80 K to 400 K during x-ray diffraction measurements. Chemical analyses of the samples were performed using a combination of a Hitachi MT3030 Plus Scanning Electron Microscope and an Oxford Energy Dispersive X-Ray Spectroscopy (EDX). Magnetic properties were measured using a Quantum Design (QD) MPMS-7 SQUID Magnetometer. Standard four-lead measurements of the electrical resistivity were carried out using a QD DynaCool PPMS System equipped with a 14-Tesla magnet. The heat capacity was measured down to 1.8 K using the PPMS.

First-principles calculations were performed using the Quantum ESPRESSO suite within the framework of density functional theory (DFT) [1]. The projector augmented wave (PAW) method

was employed alongside the Perdew-Burke-Ernzerhof (PBE) generalized gradient approximation (GGA) for exchange-correlation effects. The kinetic energy cutoff for the charge density was set to 419.8 Ry, while the wavefunction cutoff was set to 46.6 Ry, ensuring accurate total energy convergence. Brillouin zone integrations were carried out using a 6 × 9 × 3 *k*-mesh. To better capture the correlation effects in the Ir-5*d* orbitals, a Hubbard U correction of 2.0 eV was applied. pseudopotentials were sourced from Pslibrary [2]. Structural relaxation was conducted until the forces on atoms were below 4 eV/Å and the total stress was less than 5 kbar. Post processing bonding analysis was carried out using the LOBSTER (Local Orbital Basis Suite Towards Electronic-Structure Reconstruction) code [3, 4], which projects the plane-wave-based DFT wavefunctions onto a local atomic basis. This enabled the extraction of Mulliken gross populations, ICOHP, and ICOBI values, providing a detailed view of charge distribution, bonding energy, and bond order across different structural states.

II. Supplementary Figures for Lattice Parameters and DFT Calculations

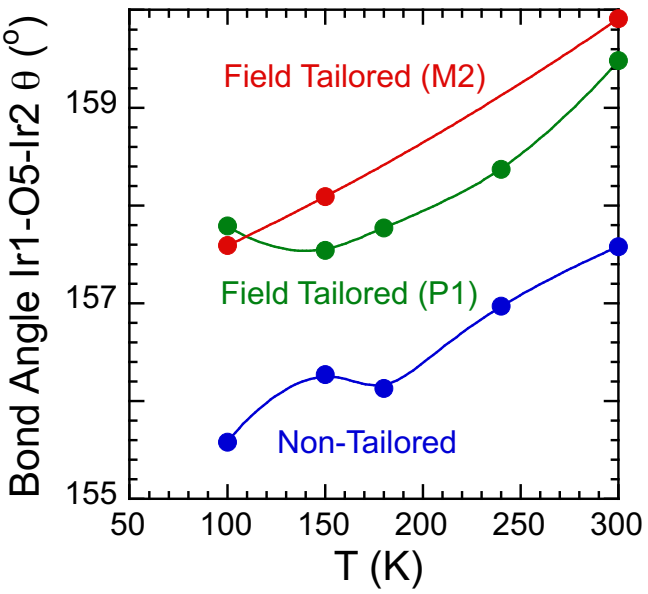

Supplementary Fig. 1. Bond angle Ir1-O5-Ir2 as a function of temperature

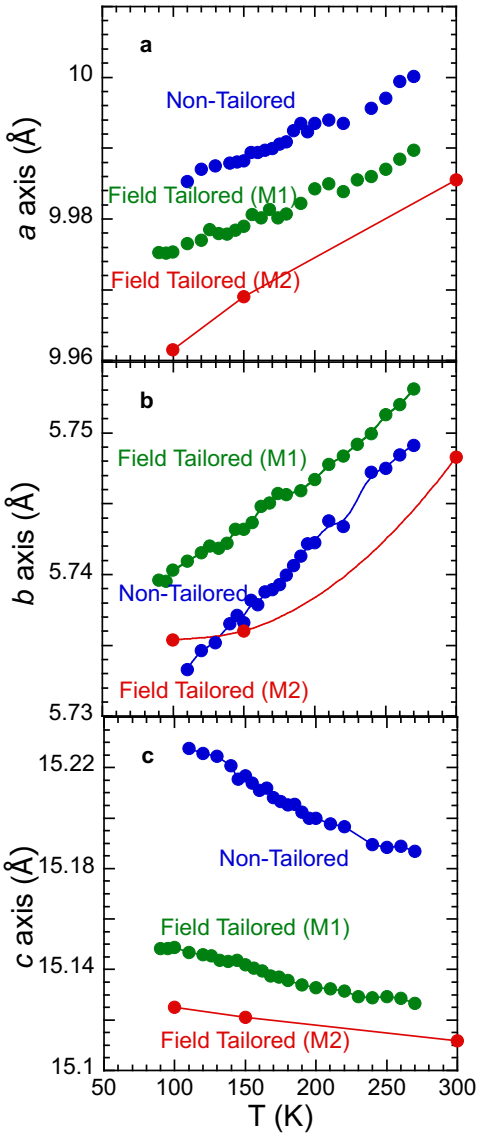

Supplementary Fig. 2. Temperature dependence of the lattice parameters (a) *a* axis, (b) *b* axis, and (c) *c* axis.

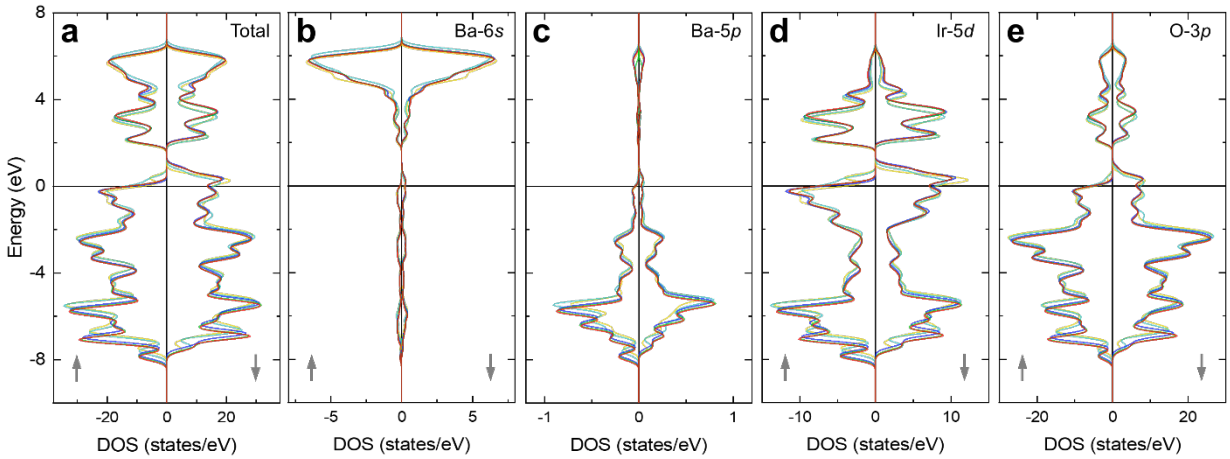

Supplementary Fig. 3. DOS of five structures: fully relaxed (yellow), position-relaxed (cyan), non-tailored (blue), field-tailored (M1) (green), and field-tailored (M2) (red).

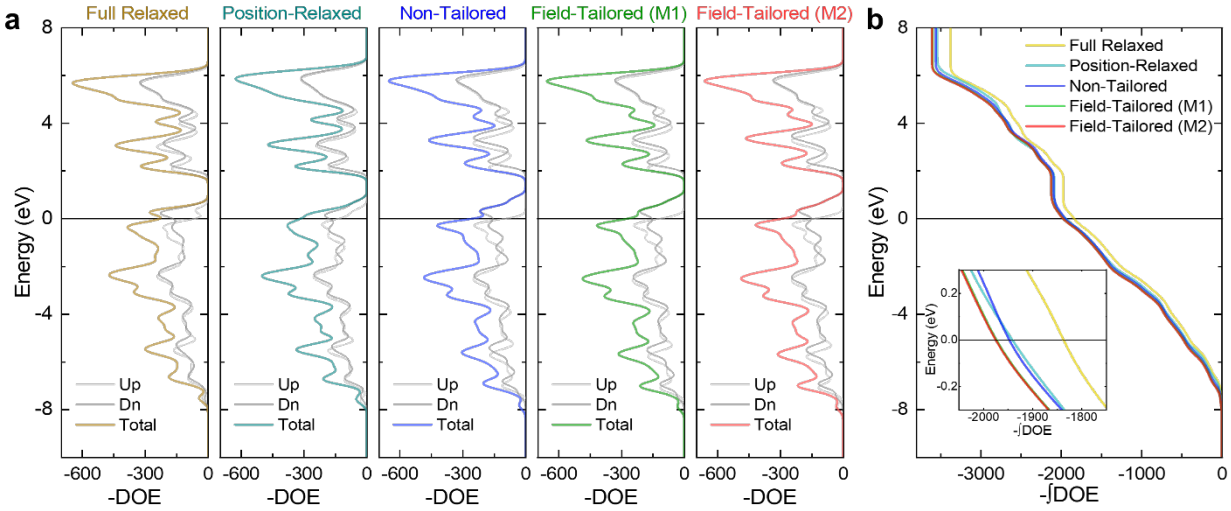

Supplementary Fig 4. (a) DOE of five structures: fully relaxed, position-relaxed, non-tailored, field-tailored (M1), and field-tailored (M2). (b) Integrated density of energy (band energy) at around Fermi level.

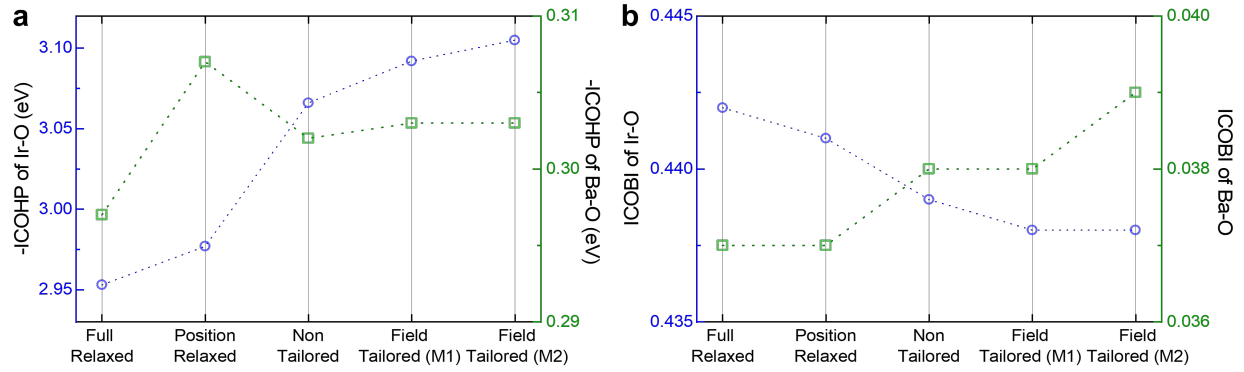

Supplementary Fig. 5. Integrated crystal orbital Hamilton population (-ICOHP) showing increases for both Ir-O and Ba-O bonds in the field-tailored structures. (b) Integrated crystal orbital bond index (ICOBI), revealing a covalent-like character for Ir-O bonds and ionic nature for Ba-O bonds, the distinct trends are in good agreement with the charge redistribution.

III. Supplementary Data on EDX and X-Ray Diffraction Analysis and Stoichiometry Confirmation

The following figures present representative energy-dispersive x-ray spectroscopy (EDX) data collected from non-tailored (T_N = 185 K), field-tailored M1 (T_N =150) and M2* (T_N ~ 0) $BaIrO_3$ single crystals. These measurements serve to confirm that the elemental ratio between Ba and Ir remains consistent across all samples, irrespective of applied field conditions during synthesis. No evidence of extrinsic impurity phases was detected within the resolution limits of the technique.

It is important to note that EDX analysis of $BaIrO_3$ can be complicated by **spectral peak overlap** between Ba and Ir. Specifically, the L-series x-ray emission lines of Ba and the M-series lines of Ir are close in energy and partially overlap. As a result, automated peak deconvolution software may incorrectly assign intensity from the Ir-M signal to the Ba-L peak, artificially elevating the apparent Ba content. This artifact is well-documented in materials containing both Ba and Ir and should not be interpreted as stoichiometric deviation or impurity incorporation.

Despite this limitation, the combined use of EDX and single-crystal x-ray diffraction provides a reliable picture: x-ray data (see **Main Text Fig. 2**, **Supplementary Figs. 1-2** and **Tables S1, S1 Extended, S2 and S2 Extended below** for representative samples) confirm single-phase crystallinity with no superstructure or secondary peaks. All these results provide strong evidence that the dramatic changes in physical properties observed in the field-tailored samples are not driven by off-stoichiometry or contamination, but instead reflect intrinsic, bulk modifications induced by magneto-synthesis.

A. EDX Spectra for Non-Tailored and Field Tailored Samples

Non-Tailored Sample (T_N ~ 185 K)

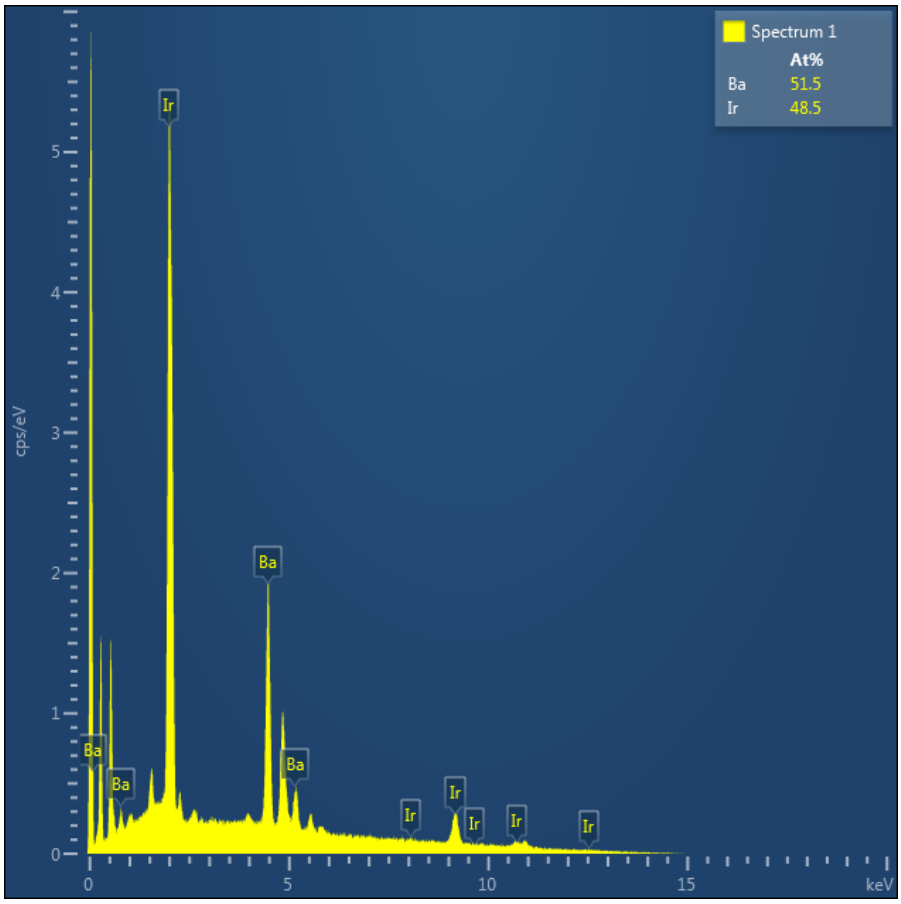

Field Tailored Sample M2* (T_N ~ 0 K)

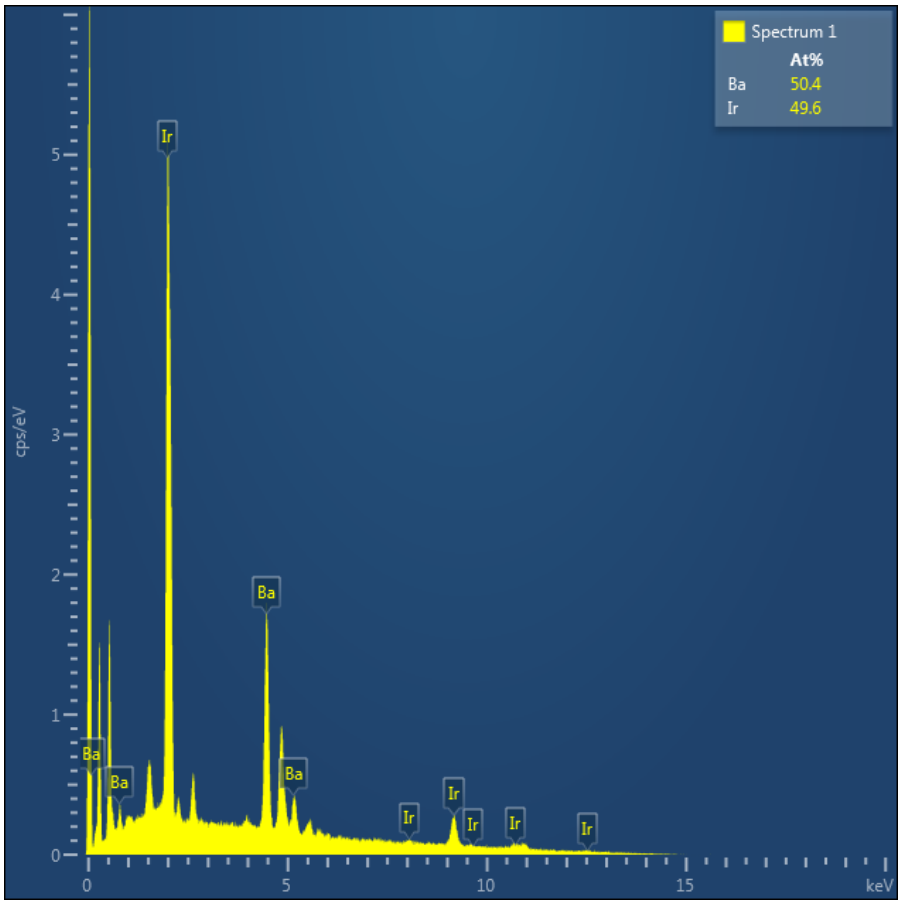

Field Tailored Sample M1 (T_N ~ 150 K)

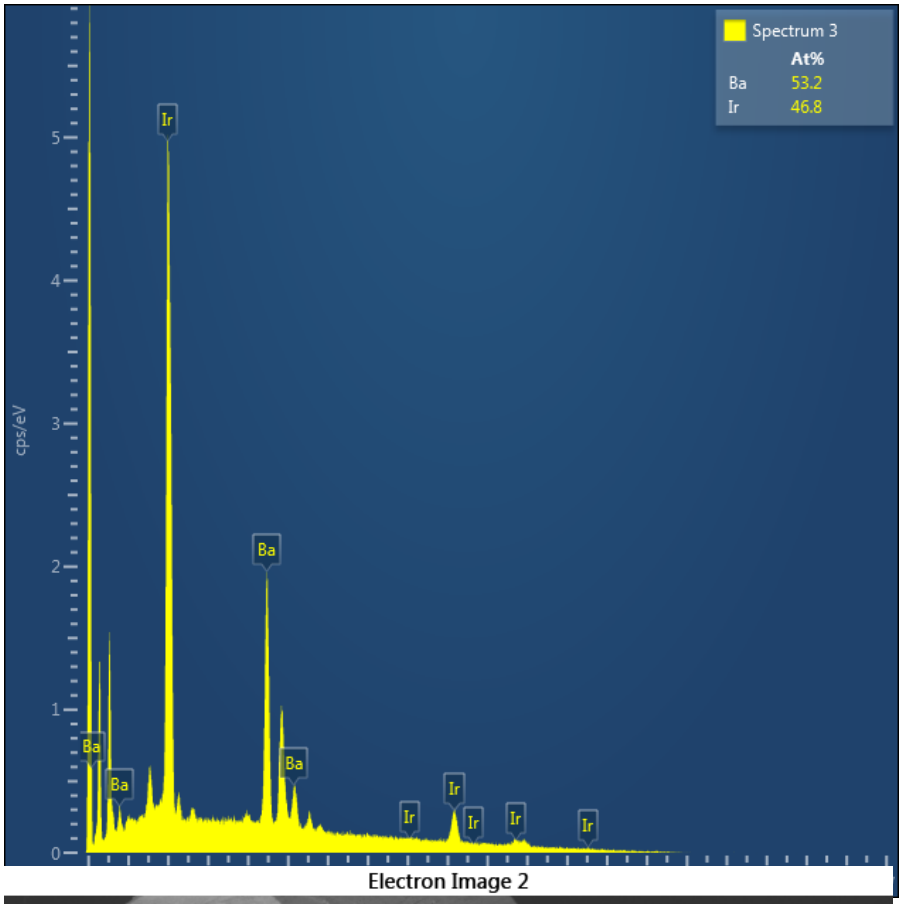

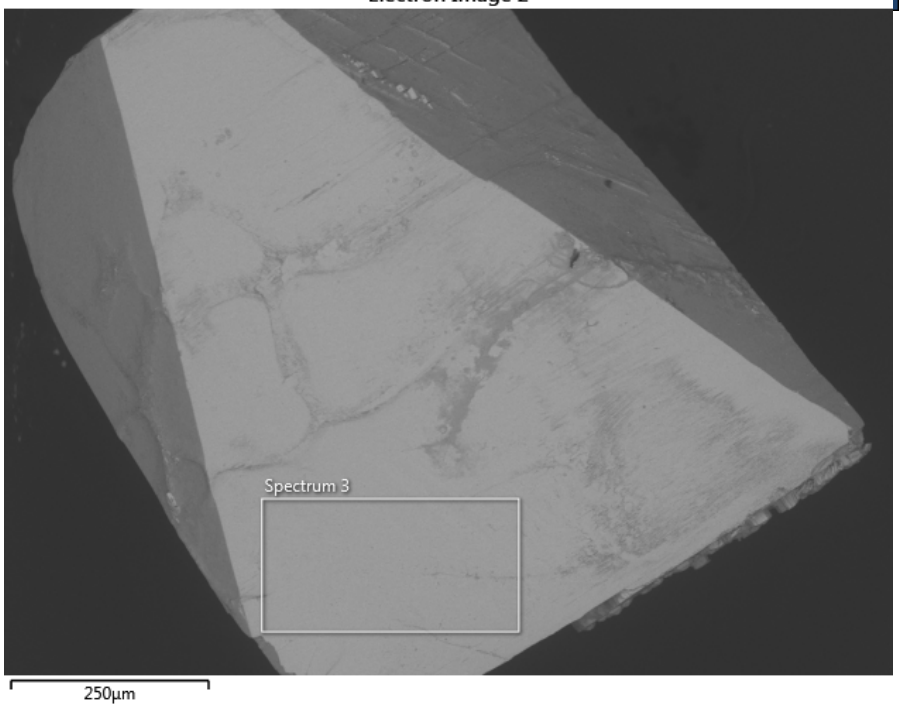

B. Tables for X-Ray Diffraction Details for Non-Tailored and Field Tailored Samples

Table S1. Single crystal diffraction results of Batch #353 (M1) in the space group *C*2/*m* at 100 K.

Empirical formula	$BaIrO_3$
Formula weight	377.54
Temperature/K	99.99
Crystal system	monoclinic
Space group	C2/m
a/Å	9.9632(4)
b/Å	5.7272(2)
c/Å	15.1501(6)
α/°	90
β/°	103.3269(14)
γ/°	90
Volume/Å^3	841.20(6)
Z	12
ρ_{calc}g/cm^3	8.943
μ/mm^{-1}	61.123
F(000)	1884.0
Radiation	MoKα (λ = 0.71073)
2Θ range for data collection/°	5.526 to 80.806
Index ranges	$-18 \le h \le 18$, $-10 \le k \le 10$, $-27 \le l \le 27$
Reflections collected	65867
Independent reflections	2876 [R_{int} = 0.0525, R_{sigma} = 0.0159]
Data/restraints/parameters	2876/0/85
Goodness-of-fit on F^2	1.203
Final R indexes [I>=2σ (I)]	R_1 = 0.0294, wR_2 = 0.0673
Final R indexes [all data]	R_1 = 0.0320, wR_2 = 0.0681
Largest diff. peak/hole / e Å^{-3}	6.81/-5.23

$R = \Sigma||F_o|-|F_c||/\Sigma|F_o|$, $wR = [\Sigma[w(|F_o|^2-|F_c|^2)^2]/\Sigma[w(|F_o|^4)]]^{1/2}$ and $w=1/(\sigma^2(I)+0.0016I^2)$

Table S1 Extended Fractional Atomic Coordinates (×10^4) and Equivalent Isotropic Displacement Parameters (Å^2×10^3) for Batch 353 (M1). U_{eq} is defined as 1/3 of the trace of the orthogonalized U_{IJ} tensor.

Atom	***x***	***y***	***z***	**U(eq)**
Ir1	4137.1(3)	0	3236.8(2)	5.41(6)
Ir2	10311.4(3)	0	1779.5(2)	5.47(6)

Atom	*x*	*y*	*z*	U(eq)
Ir3	10000	0	0	4.46(7)
Ir4	5000	0	5000	4.56(7)
Ba5	7209.8(5)	0	2514.1(3)	6.36(8)
Ba6	3497.9(5)	0	775.8(3)	6.22(8)
Ba7	1314.5(5)	0	4274.1(3)	6.97(8)
O1	10962(4)	2288(8)	966(3)	6.2(6)
O2	8591(6)	0	765(4)	6.6(9)
O3	3830(4)	-2352(8)	4165(3)	6.7(6)
O4	6086(6)	0	4016(4)	6.2(9)
O5	12071(7)	0	2720(5)	8.8(10)
O6	9456(5)	-2547(9)	2376(3)	9.8(7)

Table S1 Extended Anisotropic Displacement Parameters ($Å^2 \times 10^3$) for Batch 353 (M1). The Anisotropic displacement factor exponent takes the form: $-2\pi^2[h^2a^{*2}U_{11}+2hka^*b^*U_{12}+\ldots]$.

Atom	U_{11}	U_{22}	U_{33}	U_{23}	U_{13}	U_{12}
Ir1	5.41(11)	4.69(11)	6.08(11)	0	1.26(8)	0
Ir2	5.32(11)	4.90(11)	6.00(11)	0	0.92(8)	0
Ir3	3.94(14)	4.00(14)	5.34(14)	0	0.88(10)	0
Ir4	4.21(14)	3.77(14)	5.76(14)	0	1.26(11)	0
Ba5	5.65(16)	4.75(16)	8.67(17)	0	1.66(12)	0
Ba6	5.34(16)	4.65(16)	7.91(17)	0	-0.03(12)	0
Ba7	6.89(17)	4.89(17)	9.96(18)	0	3.64(13)	0
O1	6.9(15)	5.0(15)	6.1(15)	0.3(12)	0.5(11)	-1.5(12)
O2	3(2)	10(2)	7(2)	0	2.1(16)	0
O3	6.6(15)	5.5(16)	7.6(15)	-0.2(13)	0.7(11)	-0.8(12)
O4	2.6(19)	9(2)	8(2)	0	1.9(16)	0
O5	9(2)	10(3)	7(2)	0	0.4(18)	0
O6	12.3(18)	6.6(17)	11.8(18)	3.7(15)	5.5(14)	-0.3(14)

Table S1 Extended Bond Lengths for Batch 353 (M1)

Ir1	Ir4	2.6107(3)	Ir4	$O3^{16}$	2.024(4)
Ir1	$Ba5^{1}$	3.4810(3)	Ir4	$O3^{3}$	2.024(4)
Ir1	Ba5	3.4808(6)	Ir4	O3	2.024(5)
Ir1	$Ba5^{2}$	3.4810(3)	Ir4	O4	2.034(6)
Ir1	Ba6	3.6348(6)	Ir4	$O4^{15}$	2.034(6)
Ir1	Ba7	3.5236(6)	Ba5	$O1^{1}$	2.848(4)
Ir1	$O3^{3}$	2.021(5)	Ba5	$O1^{17}$	2.848(4)
Ir1	O3	2.021(5)	Ba5	O2	3.256(6)

Ir1	O4	2.027(6)	Ba5	$O3^{18}$	3.049(4)
Ir1	$O5^{4}$	2.027(7)	Ba5	$O3^{7}$	3.049(4)
Ir1	$O6^{2}$	1.991(5)	Ba5	O4	2.758(6)
Ir1	$O6^{5}$	1.991(5)	Ba5	$O5^{1}$	2.8874(9)
Ir2	Ir3	2.6418(3)	Ba5	$O5^{2}$	2.8874(9)
Ir2	$Ba5^{6}$	3.4707(3)	Ba5	O6	2.719(5)
Ir2	Ba5	3.5175(6)	Ba5	$O6^{3}$	2.719(5)
Ir2	$Ba5^{7}$	3.4707(3)	Ba5	$O6^{5}$	3.047(5)
Ir2	$Ba6^{7}$	3.5370(3)	Ba5	$O6^{2}$	3.047(5)
Ir2	$Ba6^{6}$	3.5370(3)	Ba6	$O1^{1}$	2.863(5)
Ir2	O1	2.006(4)	Ba6	$O1^{19}$	3.213(4)
Ir2	$O1^{3}$	2.006(4)	Ba6	$O1^{4}$	2.919(4)
Ir2	O2	2.021(6)	Ba6	$O1^{10}$	3.213(4)
Ir2	O5	1.988(7)	Ba6	$O1^{17}$	2.863(5)
Ir2	O6	2.007(5)	Ba6	$O1^{20}$	2.919(4)
Ir2	$O6^{3}$	2.007(5)	Ba6	$O2^{1}$	2.8653(2)
Ir3	$Ba6^{8}$	3.4116(5)	Ba6	$O2^{8}$	2.746(6)
Ir3	$Ba6^{6}$	3.5542(3)	Ba6	$O2^{2}$	2.8653(2)
Ir3	$Ba6^{9}$	3.4116(5)	Ba6	$O6^{2}$	2.774(5)
Ir3	$Ba6^{10}$	3.5542(3)	Ba6	$O6^{5}$	2.774(5)
Ir3	$O1^{11}$	2.033(4)	Ba7	$O3^{5}$	2.875(5)
Ir3	$O1^{12}$	2.033(4)	Ba7	$O3^{13}$	2.841(5)
Ir3	$O1^{3}$	2.033(4)	Ba7	$O3^{21}$	2.841(5)
Ir3	O1	2.033(4)	Ba7	$O3^{2}$	2.875(5)
Ir3	O2	2.016(6)	Ba7	O3	2.883(4)
Ir3	$O2^{11}$	2.015(6)	Ba7	$O3^{3}$	2.883(5)
Ir4	$Ba7^{13}$	3.4335(3)	Ba7	$O4^{15}$	3.213(6)
Ir4	$Ba7^{14}$	3.4335(3)	Ba7	$O4^{1}$	2.8921(9)
Ir4	$Ba7^{6}$	3.4335(3)	Ba7	$O4^{2}$	2.8921(9)
Ir4	$Ba7^{7}$	3.4335(3)	Ba7	$O5^{4}$	2.632(7)
Ir4	$O3^{15}$	2.024(5)			

Table S2. Single crystal diffraction results of Batch 916 (Non-Tailored) in the space group *C*2/*m* at 100 K.

Empirical formula	$BaIrO_3$
Formula weight	377.54
Temperature/K	99.65
Crystal system	monoclinic
Space group	C2/m
a/Å	9.9855(8)
b/Å	5.7314(5)
c/Å	15.2203(13)
α/°	90
β/°	103.403(4)
γ/°	90
Volume/Å^3	847.35(12)
Z	12
ρ_{calc}g/cm^3	8.878
μ/mm^{-1}	60.680
F(000)	1884.0
Radiation	MoKα (λ = 0.71073)
2Θ range for data collection/°	5.502 to 80.862
Index ranges	$-18 \leq h \leq 18$, $-10 \leq k \leq 10$, $-27 \leq l \leq 27$
Reflections collected	57470
Independent reflections	2898 [R_{int} = 0.0686, R_{sigma} = 0.0229]
Data/restraints/parameters	2898/0/85
Goodness-of-fit on F^2	1.093
Final R indexes [I>=2σ (I)]	R_1 = 0.0222, wR_2 = 0.0412
Final R indexes [all data]	R_1 = 0.0304, wR_2 = 0.0437
Largest diff. peak/hole / e Å^{-3}	3.19/-4.83

Table S2 Extended. Fractional Atomic Coordinates (×10^4) and Equivalent Isotropic Displacement Parameters (Å^2×10^3) of Batch 916 (Non-Tailored) U_{eq} is defined as 1/3 of the trace of the orthogonalised U_{IJ} tensor.

Atom	***x***	***y***	***z***	**U(eq)**
Ir1	4113.8(2)	0	3237.1(2)	3.10(4)
Ir2	10287.7(2)	0	1782.1(2)	3.11(4)
Ir3	10000	0	0	2.91(5)
Ir4	5000	0	5000	3.18(5)
Ba5	7181.9(3)	0	2515.9(2)	4.59(5)

Table S2 Extended. Fractional Atomic Coordinates ($\times 10^4$) and Equivalent Isotropic Displacement Parameters ($Å^2 \times 10^3$) of Batch 916 (Non-Tailored) U_{eq} is defined as 1/3 of the trace of the orthogonalised U_{IJ} tensor.

Atom	*x*	*y*	*z*	U(eq)
Ba6	3488.0(3)	0	779.2(2)	4.40(5)
Ba7	1307.2(3)	0	4280.9(2)	4.68(5)
O1	10945(3)	2289(5)	970.5(19)	5.3(4)
O2	8584(4)	0	751(3)	5.0(6)
O3	3820(3)	-2352(5)	4168.2(19)	5.7(4)
O4	6064(4)	0	4009(3)	5.9(6)
O5	12034(4)	0	2744(3)	6.2(6)
O6	9411(3)	-2546(5)	2368(2)	7.1(5)

Table S2 Extended. Anisotropic Displacement Parameters ($Å^2 \times 10^3$) for Batch 916 (Non-Tailored). The Anisotropic displacement factor exponent takes the form: $-2\pi^2[h^2a^{*2}U_{11}+2hka^*b^*U_{12}+\ldots]$.

Atom	U_{11}	U_{22}	U_{33}	U_{23}	U_{13}	U_{12}
Ir1	3.01(7)	3.00(7)	3.44(7)	0	1.08(5)	0
Ir2	2.74(7)	3.17(7)	3.45(7)	0	0.83(5)	0
Ir3	2.66(9)	3.19(10)	2.97(10)	0	0.86(7)	0
Ir4	2.76(10)	3.01(10)	3.88(10)	0	1.00(7)	0
Ba5	3.96(10)	4.01(11)	6.08(11)	0	1.74(8)	0
Ba6	3.85(11)	3.79(11)	5.25(11)	0	0.45(8)	0
Ba7	5.03(11)	3.89(11)	5.83(11)	0	2.73(9)	0
O1	8.4(11)	3.9(11)	4.1(10)	-1.2(8)	2.3(8)	-2.4(8)
O2	4.7(15)	8.1(16)	2.0(14)	0	0.4(11)	0
O3	7.2(11)	6.0(11)	3.7(10)	0.6(9)	0.7(8)	-1.7(8)
O4	5.5(15)	7.9(16)	4.9(15)	0	2.5(11)	0
O5	3.8(14)	8.9(17)	5.2(15)	0	-0.5(11)	0
O6	8.5(11)	4.8(11)	8.5(12)	3.1(9)	2.8(9)	-0.5(9)
Ir1	3.01(7)	3.00(7)	3.44(7)	0	1.08(5)	0

Table S2 Extended. Bond Lengths for Batch 916 (Non-Tailored)

Atom	Atom	Length/Å	Atom	Atom	Length/Å
Ir1	Ir4	2.6234(3)	Ir4	O3	2.029(3)
Ir1	$Ba5^1$	3.4867(3)	Ir4	$O3^{15}$	2.029(3)
Ir1	Ba5	3.4856(4)	Ir4	$O3^{16}$	2.029(3)
Ir1	$Ba5^2$	3.4867(3)	Ir4	O4	2.036(4)

Table S2 Extended. Bond Lengths for Batch 916 (Non-Tailored)

Ir1	Ba6	3.6472(5)	Ir4	O4[16]	2.036(4)
Ir1	Ba7	3.5274(4)	Ba5	O1[1]	2.851(3)
Ir1	O3	2.026(3)	Ba5	O1[17]	2.851(3)
Ir1	O3[3]	2.026(3)	Ba5	O2	3.305(4)
Ir1	O4	2.028(4)	Ba5	O3[18]	3.065(3)
Ir1	O5[4]	2.038(4)	Ba5	O3[7]	3.065(3)
Ir1	O6[2]	2.000(3)	Ba5	O4	2.755(4)
Ir1	O6[5]	2.000(3)	Ba5	O5[1]	2.8946(7)
Ir2	Ir3	2.6605(3)	Ba5	O5[2]	2.8946(7)
Ir2	Ba5[6]	3.4724(3)	Ba5	O6	2.714(3)
Ir2	Ba5	3.5315(4)	Ba5	O6[3]	2.714(3)
Ir2	Ba5[7]	3.4724(3)	Ba5	O6[5]	3.065(3)
Ir2	Ba6[7]	3.5356(3)	Ba5	O6[2]	3.065(3)
Ir2	Ba6[6]	3.5356(3)	Ba6	O1[1]	2.861(3)
Ir2	O1	2.013(3)	Ba6	O1[19]	3.244(3)
Ir2	O1[3]	2.013(3)	Ba6	O1[4]	2.932(3)
Ir2	O2	2.030(4)	Ba6	O1[9]	3.244(3)
Ir2	O5	2.000(4)	Ba6	O1[17]	2.861(3)
Ir2	O6	2.013(3)	Ba6	O1[20]	2.932(3)
Ir2	O6[3]	2.013(3)	Ba6	O2[1]	2.8680(3)
Ir3	Ba6[8]	3.4092(4)	Ba6	O2[10]	2.733(4)
Ir3	Ba6[9]	3.5677(3)	Ba6	O2[2]	2.8680(3)
Ir3	Ba6[6]	3.5677(3)	Ba6	O6[2]	2.764(3)
Ir3	Ba6[10]	3.4092(4)	Ba6	O6[5]	2.764(3)
Ir3	O1[11]	2.036(3)	Ba7	O3[5]	2.882(3)
Ir3	O1[12]	2.036(3)	Ba7	O3[13]	2.834(3)
Ir3	O1[3]	2.036(3)	Ba7	O3[21]	2.834(3)
Ir3	O1	2.036(3)	Ba7	O3[2]	2.882(3)
Ir3	O2	2.014(4)	Ba7	O3	2.888(3)
Ir3	O2[11]	2.014(4)	Ba7	O3[3]	2.888(3)
Ir4	Ba7[13]	3.4317(3)	Ba7	O4[16]	3.240(4)
Ir4	Ba7[14]	3.4317(3)	Ba7	O4[1]	2.8975(7)
Ir4	Ba7[6]	3.4317(3)	Ba7	O4[2]	2.8975(7)
Ir4	Ba7[7]	3.4317(3)	Ba7	O5[4]	2.605(4)
Ir4	O3[3]	2.029(3)			

IV. Supplementary Data on Reproducibility of Magnetic Behavior Across Batches

To further support the intrinsic nature of the field-induced transformations observed in $BaIrO_3$, we present additional *a*- and *c*-axis magnetic susceptibility χ_a and χ_c data collected from independently grown crystals corresponding to the M1, M2, and M2* synthesis conditions. These measurements were performed on multiple batches synthesized under identical magnetic field protocols. The results confirm the high reproducibility of the magnetic behavior reported in the main text, including the systematic suppression of the Néel temperature T_N with increasing synthesis field strength. The close agreement across samples rules out sample-specific anomalies or stochastic impurity effects, reinforcing the conclusion that the observed phenomena are robust consequences of magneto-synthesis.

A. Grown Crystals at the M1 Synthesis Conditions

Supplementary Fig. 6:

The *a*-axis magnetic susceptibility χ_a for two different samples from **Batch #353 (M1)**:

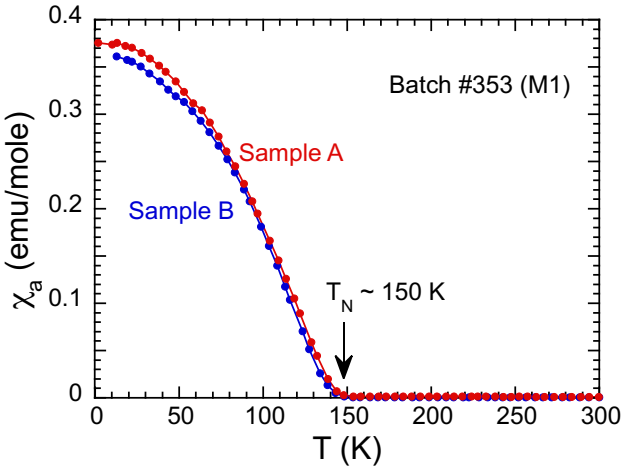

Supplementary Fig. 7:

The *c*-axis magnetic susceptibility χ_c for two different samples from **Batches #361 and 424 (M1)**:

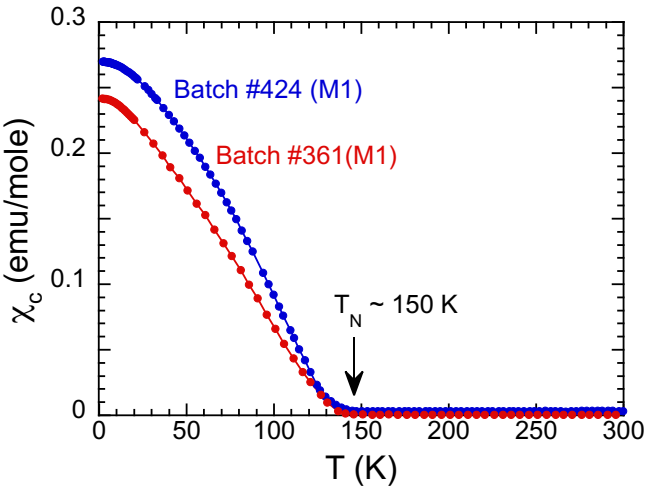

B. Grown Crystals at the M2 Synthesis Conditions

Supplementary Fig. 8:

The *a*-axis magnetic susceptibility χ_a for two different samples from **Batch #480 (M2)**:

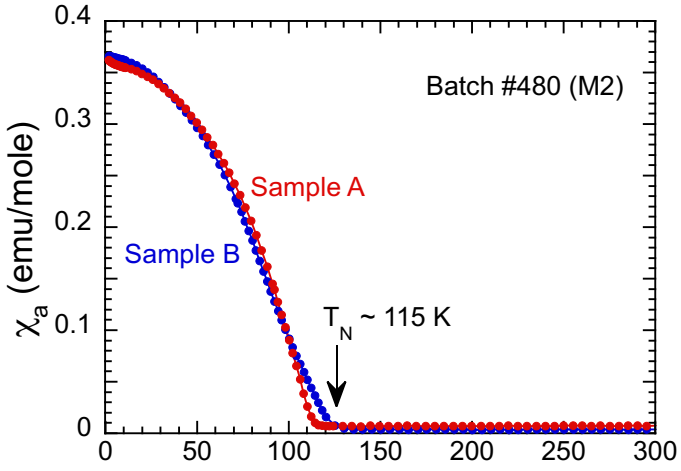

Supplementary Fig. 9:

The *c*-axis magnetic susceptibility χ_a for a sample from **Batch #469 (M2)**:

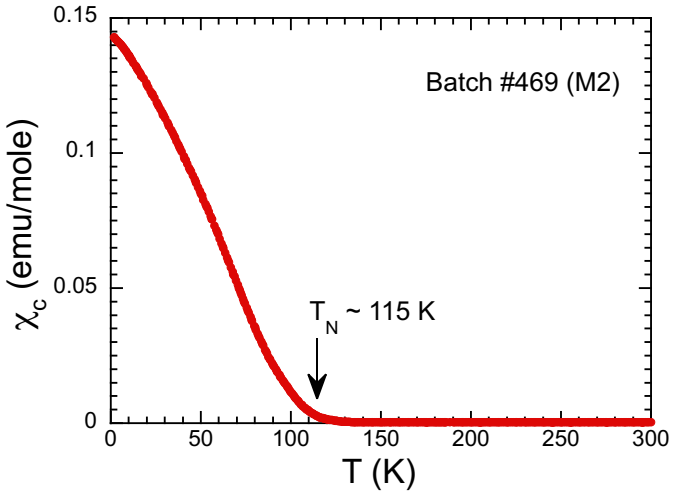

C. Grown Crystals at the M2* Synthesis Conditions

Supplementary Fig. 10:

The *c*-axis magnetic susceptibility χ_a for a sample from **Batch #470 (M2*)**:

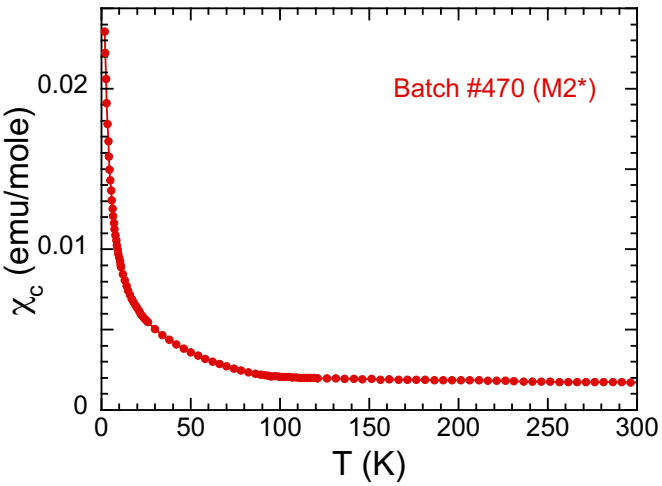

References

1. *Advanced capabilities for materials modelling with Quantum ESPRESSO*, Giannozzi, Paolo, et al. Journal of physics: Condensed matter 29.46 465901. (2017)
2. https://github.com/dalcorso/pslibrary
3. *LOBSTER: A tool to extract chemical bonding from plane-wave based DFT*, Journal of Computational Chemistry, 1030-1035, (2016)
4. *LOBSTER: Local orbital projections, atomic charges, and chemical-bonding analysis from projector-augmented-wave-based density-functional theory*, Journal of computational chemistry 41.21, 1931-1940. (2020)